Earth Planet. Sci. Lett. 658 (2025) 119324

Contents lists available at ScienceDirect

Earth and Planetary Science Letters

journal homepage: www.elsevier.com/locate/epsl

2023–2024 inflation-deflation cycles at Svartsengi and repeated dike injections and eruptions at the Sundhnúkur crater row, Reykjanes Peninsula, Iceland

Michelle Parks [a,*], Vincent Drouin [a], Freysteinn Sigmundsson [b], Ásta R. Hjartardóttir [a], Halldór Geirsson [b], Gro B.M. Pedersen [a], Joaquin M.C. Belart [c], Sara Barsotti [a], Chiara Lanzi [a], Kristín Vogfjörd [a], Andrew Hooper [d], Benedikt Ófeigsson [a], Sigrún Hreinsdóttir [e], Einar Bessi Gestsson [a], Ragnar H. Þrastarson [a], Páll Einarsson [b], Valentyn Tolpekin [f], Drew Rotheram-Clarke [g], Sydney R. Gunnarsson [c], Birgir V. Óskarsson [c], Virginie Pinel [h]

[a] Icelandic Meteorological Office, Reykjavík, Iceland
[b] Nordic Volcanological Center, Institute and Faculty of Earth Sciences, University of Iceland, Reykjavík, Iceland
[c] Natural Science Institute of Iceland, Reykjavík, Iceland
[d] COMET, School of Earth and Environment, University of Leeds, Leeds, United Kingdom
[e] GNS Science, Lower Hutt, New Zealand
[f] ICEYE Oy, Espoo, Finland
[g] Geological Survey of Canada, Pacific Division, Vancouver, British Columbia, Canada
[h] Univ. Grenoble Alpes, Univ. Savoie Mont Blanc, CNRS, IRD, Univ. Gustave Eiffel, ISTerre, Grenoble, France

ARTICLE INFO

Edited by J.P. Avouac.

Keywords:
Svartsengi volcanic system
Sundhnúkur volcanic eruptions
Repeated dike intrusions
Inflation-deflation cycles
Eruption forecasting
Reykjanes Peninsula

ABSTRACT

Series of inflation-deflation cycles have occurred during 2020–2024 in the center of the Svartsengi volcanic system, SW-Iceland. Since 27 October 2023, continuous inflation has been interrupted by deflation periods when nine dike injections and seven eruptions have occurred from 10 November 2023 to 8 December 2024 at the Sundhnúkur crater row and its extension. Extensive observations of ground deformation using GNSS (Global Navigation Satellite System) geodesy and interferometric analysis of synthetic aperture satellite (InSAR) images is here used to improve understanding of the dynamics of magma accumulation and transfer, both prior to and during repeated rifting events. Joint inversions of the GNSS and InSAR data, considering a deformation source within a uniform elastic half-space, infer pressure changes at about 4–5 km depth near the regional brittle-ductile boundary, with inflow causing volume increase rates of 2.4–9 m^3/s. Geodetic modelling using GNSS has been undertaken in near real-time throughout the events, using deformation sources in fixed locations inferred in earlier joint inversions. The deflation periods began rapidly when a dike propagated from the eastern edge of the magma accumulation area. The estimated volume of dikes is in the range (1–133) $\times 10^6$ m^3, with the first event being by far the largest and longest (~15 km). Geodetic observations have contributed to success in forecasting diking/eruption onset in the medium and short term, using the expectation that a correlation exists between volume loss in the magma domain during a deflation event and subsequent volume recharge to the system before the next event is triggered.

1. Introduction

Volcanic activity on the Reykjanes Peninsula oblique spreading plate boundary in southwest Iceland (Fig. 1) is highly episodic. Geological observations have resolved activity during the last few thousand years. Volcano-tectonic phases last a few hundred years, with multiple eruptions occurring over a broad area on the peninsula, followed by non-eruptive periods of about 800–1000 years (Sæmundsson et al., 2020).

* Corresponding author.
E-mail address: michelle@vedur.is (M. Parks).

https://doi.org/10.1016/j.epsl.2025.119324
Received 13 November 2024; Received in revised form 9 February 2025; Accepted 12 March 2025
Available online 23 March 2025

Historical accounts are also important for unravelling the style of volcanic activity; the Reykjanes Fires activity phase from 800 to 1240 CE (Sæmundsson et al., 2010; Sigurgeirsson, 2023) commenced shortly before the time of settlement in Iceland, followed by a non-eruptive period until 2021. Lava fields cover a large part of the Reykjanes Peninsula and normal faulting and fractures are widespread (e.g., Clifton and Kattenhorn, 2006), grouping into fissure swarms. Central volcanoes are not well developed. The extent of high-temperature geothermal fields has been inferred from resistivity measurements (Flóvenz et al., 2022). The main crater rows of the Svartsengi system, the Eldvörp and Sundhnúkur crater rows (Jenness and Clifton, 2009), are on each side of the Svartsengi geothermal field, respectively, suggesting a broad heat source between them (Fig. 1). Studies using seismic ambient-noise surface wave tomography find a significant low-velocity anomaly at ~3–6 km depth under the Svartsengi system, interpreted as due to anelasticity of the brittle-ductile transition zone, combined

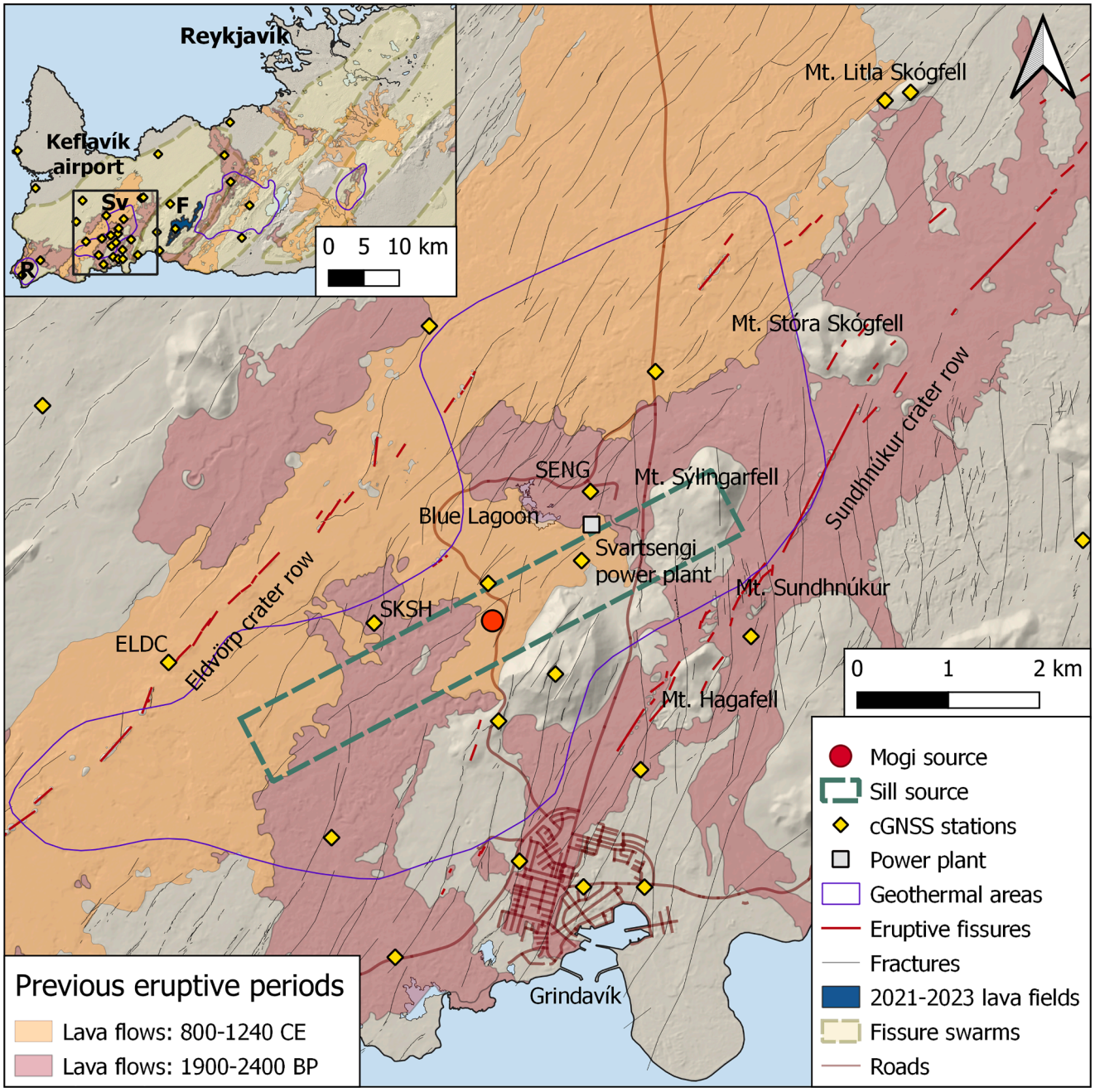

Fig. 1. Map of the central part of the Svartsengi volcanic system and the town of Grindavík, with lava flows (Sæmundsson et al., 2010) from two prior eruptive periods: (i) 800–1240 CE overlapping with the initial settlement of Iceland that began around 870 CE, (ii) the period before that occurred around 1900–2400 years BP. Also shown are fractures (Clifton and Kattenhorn, 2006; Ducrocq et al., 2024) and old eruptive fissures (from Clifton and Kattenhorn, 2006). Inset shows the location of the Svartsengi (Sv) volcanic system on the Reykjanes Peninsula in SW-Iceland. To the west of it is the Reykjanes (R) volcanic system, and to the east is the Fagradalsfjall (F) volcanic system where eruptions occurred between 2021 and 2023 (lava from these years shown as dark grey shading). Fissure swarms are after Jóhannesson and Sæmundsson (2009). Outline of high-temperature geothermal areas according to resistivity measurements from Flóvenz at al. (2022). The inset and main map also show locations of GNSS sites with stations SKSH, ELDC and SENG indicated (see Fig. 3 & Supplementary Fig. S1), and the surface projections of average locations of point source (Mogi, 1958) and horizontal rectangular sill (Okada, 1992) derived from joint GNSS-InSAR inversions spanning uplift episodes and used as fixed source locations in the automated GNSS inversions.

with the high temperatures of the geothermal fields, possibly with some amount of partial melt (Dalkhani et al., 2024; Martins et al., 2020).

Regional deformation on the Reykjanes Peninsula until end of 2019 was dominated by plate boundary strain due the oblique spreading of the Eurasian and North-American plate boundary of ~19 mm/yr in direction N104°E, with a central plate boundary axis in the southern-to-middle part of the peninsula (Sturkell et al., 1994; Hreinsdóttir et al., 2001; Keiding et al., 2008; Sigmundsson et al., 2020). The plate boundary zone was found to subside regionally by up to ~6 mm/yr (Vadon and Sigmundsson, 1997), with additional localized subsidence due to heat and electricity production in the Reykjanes and Svartsengi geothermal systems causing localized subsidence on the centimeter scale (e.g., Keiding et al., 2010, Parks et al., 2020). The third main geothermal system on the peninsula, Krýsuvík, showed inflation-deflation episodes between 2007 and 2016 (Guðjónsdóttir et al., 2020). Co-seismic deformation related to earthquakes up to M5.6 has been observed on the peninsula (e.g., Pagli et al., 2003). The seismicity of the Reykjanes Peninsula oblique rift is summarized by Björnsson et al. (2020) and Einarsson (2008). Following the active volcanic period that ended in 1240 CE, the seismic activity appears to have been very low. No earthquakes are documented until 1724 CE. The activity since has been episodic, with high activity in 1900–1910, 1924–1935, 1967–1973, 1998–2013 and 2017. The largest earthquakes in the latest episodes are known to have been associated with strike-slip faulting (e.g. Einarsson, 1991; Árnadóttir et al., 2004; Antonioli et al., 2006). Deformation along the plate boundary during these decades appears to have been accommodated by strike-slip faulting. At Svartsengi, there is no evidence of magmatic contribution, such as inflation sources, volcanic tremor, or earthquake swarms propagating along the fissure swarm, until January 2020.

After a quiet period of 781 years with no eruptions, volcano-tectonic reactivation of the Reykjanes Peninsula commenced in December 2019, with a week-long microearthquake swarm beneath Fagradalsfjall at depths between 3 and 7 km. The first clear sign of new magma migration beneath the peninsula was detected on 21 January 2020 – with a strong increase in seismicity and crustal deformation marking the beginning of the first uplift period in the Svartsengi area, indicative of pressure increase within the crust. The first diking and eruptive activity in the ongoing active period was, however, 10 km farther east in the Fagradalsfjall area, where diking occurred from 24 February until 19 March 2021, when an eruption began (Sigmundsson et al., 2022). From February 2021 until August 2023, four dike intrusions and three eruptions occurred there (Parks et al., 2023; Pedersen et al., 2022). The inferred initial magma inflow rate into the first dike was 30–35 m^3/s which reduced to <10 m^3/s prior to the eruption onset. The initial dike intrusion triggered over 20,000 recorded earthquakes across the peninsula, including over 60 events with magnitudes $M_W>4$, and six $M_W>5$. For the three eruptions in the Fagradalsfjall area (2021, 2022, 2023), the inferred inflow rate to the dike immediately before eruption onset and the initial lava extrusion rate were found to be about equal. This flow rate was used to assess the hazard associated with lava flows (Parks et al., 2023; Pedersen et al., 2022; Barsotti et al., 2023). Petrochemical studies have revealed that in the 2021 eruption, the shallowest depth at which magma equilibrated before eruption is near the crust-mantle boundary around 15 km depth, with different types of basaltic magma from the mantle then tapped during the eruption (Halldórsson et al., 2022).

At Svartsengi, the initial period of uplift in January 2020, was followed by uplift periods in March-April, May-July 2020, and in May-June 2022 (Cubuk-Sabuncu et al., 2021; Geirsson et al., 2021; Sigmundsson et al., 2024). All of these occurred without eruptions. After an eruption in Fagradalsfjall volcanic system between 10 July-5 August 2023, the focus of activity shifted to the Svartsengi volcanic system. Confirmed inflation (detectable uplift) began on 27 October 2023 (Sigmundsson et al., 2024), with seismicity increasing 1–2 days before. Rapid inflation continued until 10 November 2023 when a major rifting event occurred, with the emplacement of an inferred 15 km long dike (Sigmundsson et al., 2024). Extensive graben formation and destruction occurred in the town of Grindavík (De Pascale et al., 2024). The rifting event triggered over 20,000 recorded earthquakes across the peninsula, including over 40 $M_W>4$ events, and two $M_W>5$, the largest being $M_W5.2$. Most of the seismicity was in the vicinity of the dike.

The crustal volume where magma accumulates in the Svartsengi area has been inferred to lie at 4–5 km depth, referred to as the Svartsengi magma domain, comprising liquid magma, magma mush and hot solid rock (Sigmundsson et al., 2024). Magma is being rapidly injected into dike intrusions when a critical pressure is reached, and the boundary of the magma domain fails. Geodetic data and modelling indicate that the five inflation episodes that occurred in this area between 21 January 2020 - 10 November 2023 were injections of magma into an extensive pre-existing magma domain (Sigmundsson et al., 2024). Its areal extent has been inferred to be broad, spanning from close to the Eldvörp crater row in the west to the Sundhnúkur crater row in the east – and lies beneath the Blue Lagoon and Svartsengi power plant (Sigmundsson et al., 2024; this study).

Following the initial rifting event in the Svartsengi volcanic system, eight dike intrusions and seven eruptions have occurred (Table 1), in the vicinity of the Sundhnúkur crater row, extending into the town of Grindavík (Fig. 2), the most recent of which occurred in November 2024. The petrochemistry of the eruptive products from the first four eruptions have been interpreted to show evidence for a dynamic mid-crustal magma domain, with unusual geochemical heterogeneity due to substantial mantle-derived geochemical variability, that can be interpreted in terms of magma being stored in separate lenses within the magma domain (Matthews et al., 2024).

The main aim of this study is to improve understanding of: i) magma accumulation prior to diking events and eruptions, ii) the style of magma transfer in repeated such events, iii) evolution of volume changes in an underlying magma domain in relation to inflation-deflation cycles, and iv) evaluate implications for forecasting diking events and eruptions. For that purpose, we use our extensive geodetic dataset to evaluate all the inflation-deflation cycles that occurred in the Svartsengi area between 27 October 2023 and December 2024, and the diking events and eruptions following the 10 November 2023 rifting event. A dike model for that initial event is presented by Sigmundsson et al. (2024).

2. Methods

2.1. Seismicity

Seismicity in Iceland is monitored by the Icelandic Metorological Office's (IMO) national seismic network, Veðurstofa íslands (VI) and automatically located by the South Iceland Lowlands (SIL) analysis system (Böðvarsson et al., 1999). Since 2020, the monitoring network on the Reykjanes Peninsula has included ~20 stations, around half of which are owned by IMO's collaborators (see acknowledgements). Earthquake detections and locations have been substantially improved by this augmentation of the network. Routine processing of seismicity involves manual reviewing and improvements of the automatic locations and calculation of local magnitudes (Rögnvaldsson and Slunga, 1993). These magnitudes can be somewhat underestimated for the larger events. A temporary version of the SIL national earthquake catalogue is accessible at: https://skjalftalisa.vedur.is. A harmonized, quality checked version of the SIL catalogue is in progress, soon to be made available in the earthquake-list service of the Volcano Observations Thematic Core Service (VOLC-TCS) on the European Plate Observatory's (EPOS) Data Portal. Moment magnitudes (M_W) of the largest events are also automatically calculated specifically from attenuation relations for Peak Ground Velocity (PGV) in Iceland (Pétursson and Vogfjörd, 2009). These magnitudes are openly available in the Shakemap service of the VOLC-TCS on the EPOS Data Portal

Table 1
Overview of diking events and eruptions that occurred between November 2023 and December 2024. Volumes displayed are median values ± one standard deviation, derived from joint InSAR-GNSS inversions. The values displayed for the 10 November dike (event 1) are from Sigmundsson et al. (2024). Data displayed for events 2 to 9 were derived during this study.

Event number	Dates of diking	Start time of diking	Duration of diking (hours)	Repose (days)	Eruptive period	Eruption length (days)	Volume loss of magma domain ($\times 10^6$ m^3)	Dike volume ($\times 10^6$ m^3)	Average inflow rate to dike (m^3/s)
1	10.11.2023 to 11.11.2023	16:55	14.9	NA	NA	NA	77.8 ± 1.2	132.7 ± 2.2	2482
2	18.12.2023 to 19.12.2023	20:47	4.5	37	18.12.2023 to 21.12.2023	3	10.6 ± 0.3	9.9 ± 0.9	618
3	14.1.2024	02:55	5.5	24	14.1.2024 to 16.1.2024	2	10 ± 0.5	21.1 ± 0.5	1062
4	8.2.2024	05:07	2.4	23	08.2.2024 to 9.2.2024	1	6.7 ± 0.3	3.4 ± 0.1	391
5	2.3.2024	14:37	3.6	22	NA	NA	2 ± 0.7	2.6 ± 0.4	201
6	16.3.2024	19:29	1.3	14	16.3.2024 to 8.5.2024	53	6.9 ± 0.5	1.4 ± 0.8	295
7	29.5.2024	10:42	3.4	21	29.5.2024 to 22.6.2024	24	12.7 ± 0.6	4.1 ± 0.1	335
8	22.8.2024 to 23.8.2024	20:48	7.1	61	22.8.2024 to 5.9.2024	14	19.7 ± 0.4	6 ± 0.1	235
9	20.11.2024 to 21.11.2024	22:20	1.8	76	20.11.2024 to 8.12.2024	18	12.8 ± 0.3	0.9 ± 0.1	140

Note. For the 18 December 2023 diking event the geodetic inversion spanned the time period 11–20 December 2023, based on available input interferograms. The calculated volume decrease in the magma domain is 7.7 million m^3 during this time period. As this inversion included 7 days of pre-diking inflation, the volume loss in the magma domain during this diking event was underestimated. We fixed the GNSS time series of volume change (Figs. 6 & Supplementary Figure S3) between 11 and 20 December 2023 to match this same amount derived from the joint inversion. We then used the volume loss calculated from the time series between 18 and 20 December 2023, to estimate the actual volume loss in the magma domain during this diking event.

(https://www.ics-c.epos-eu.org/). Earthquake magnitudes shown in Fig. 3 are from the temporary local catalogue.

2.2. GNSS

We use Global Navigation Satellite System (GNSS) geodesy to infer three-dimensional displacements. Methodology and analyses of seismic and GNSS data are similar as those used by Parks et al. (2023) and Sigmundsson et al. (2024). GNSS data used here was collected at 37 continuously recording stations (cGNSS), displayed in Fig. 1. The GNSS data was analyzed using the GAMIT/GLOBK 10.7 software (Herring et al., 2018), estimating 24 hr site positions in the ITRF08 reference frame (Altamimi et al., 2012). We solve for daily site positions and satellite orbits, constraining the position of global reference stations. We correct for ocean loading using the FES2004 model (Lyard et al., 2006) and use IGS08 azimuth and elevation dependent absolute phase centre model for all antennas.

2.3. InSAR

Interferometric analysis of imagery from six SAR satellite missions: Sentinel-1, COSMO-SkyMed, ICEYE, SAOCOM, RADARSAT (RCM), and TerraSAR-X was used to create interferograms showing line-of-sight (LOS) change in distance from ground to satellite. Interferograms were generated using the standard two-pass interferometry procedure. The Sentinel-1, COSMO-SkyMed, SAOCOM, and TerraSAR-X datasets were processed at IMO while the ICEYE and RADARSAT datasets were processed at ICEYE and the Geological Survey of Canada, respectively (for more details about processing see Supplementary Text S1). For each event (dike intrusion, inflation episode), the best interferograms were selected based on their time coverage of the event and the quality of their phase information. Lava fields formed during the new eruptions and the 2021–2023 Fagradalsfjall lava fields were masked to avoid introducing false deformation signals in the modelling caused by topographic error or lava cooling.

2.4. Photogrammetry

Photogrammetry was used to create digital elevation models (DEMs) using similar approaches as described by Pedersen et al. (2022) and Gouhier et al. (2022). Co-registration of DEMs and evaluation of differences was done using the method of Nuth and Kaab (2011), to minimize horizontal and vertical biases between the two datasets. Graben boundary faults used in geodetic modelling were mapped using the difference in elevation between two digital elevation DEMs, based on data acquired on 19 November 2023 using the Pléiades satellite and 13 February 2024 using airborne photogrammetry. The total bulk volume of erupted lavas was obtained by comparing DEMs acquired from airplane photogrammetric surveys on 2 November 2023 (pre-eruptions), 30 September 2024 (after six of the seven eruptions) and 13 December 2024. For more details regarding the data processing see Supplementary Text S2.

2.5. Geodetic modelling

Three-dimensional ground displacements inferred from cGNSS and LOS displacements from InSAR were used as input for geodetic modelling. Observed ground deformation was compared to predicted surface deformation from simple sources of deformation, embedded within a uniform elastic half-space. The ground deformation patterns during diking events can be explained by a single source of magma withdrawal and a subvertical dike. Inflation can be explained by single source of magma accumulation, modelled using either a point source of pressure model (Mogi, 1958) or opening on a rectangular plane (Okada, 1992). Both inflation and deflation events have been constrained using joint inversion of the InSAR and GNSS data. During diking events we endeavored to use short-period interferograms (spanning 1–2 days where possible). The joint inversions utilized a modified version of the GBIS geodetic Bayesian inversion software (Bagnardi and Hooper, 2018). Automated modelling to obtain the time-series of volume change within the Svartsengi magma domain was undertaken using IMO in-house software and utilizes only GNSS data from 24-hour solutions. This model was run for both the point source of pressure and a rectangular sill source. As the geodetic data show that inflation deformation is

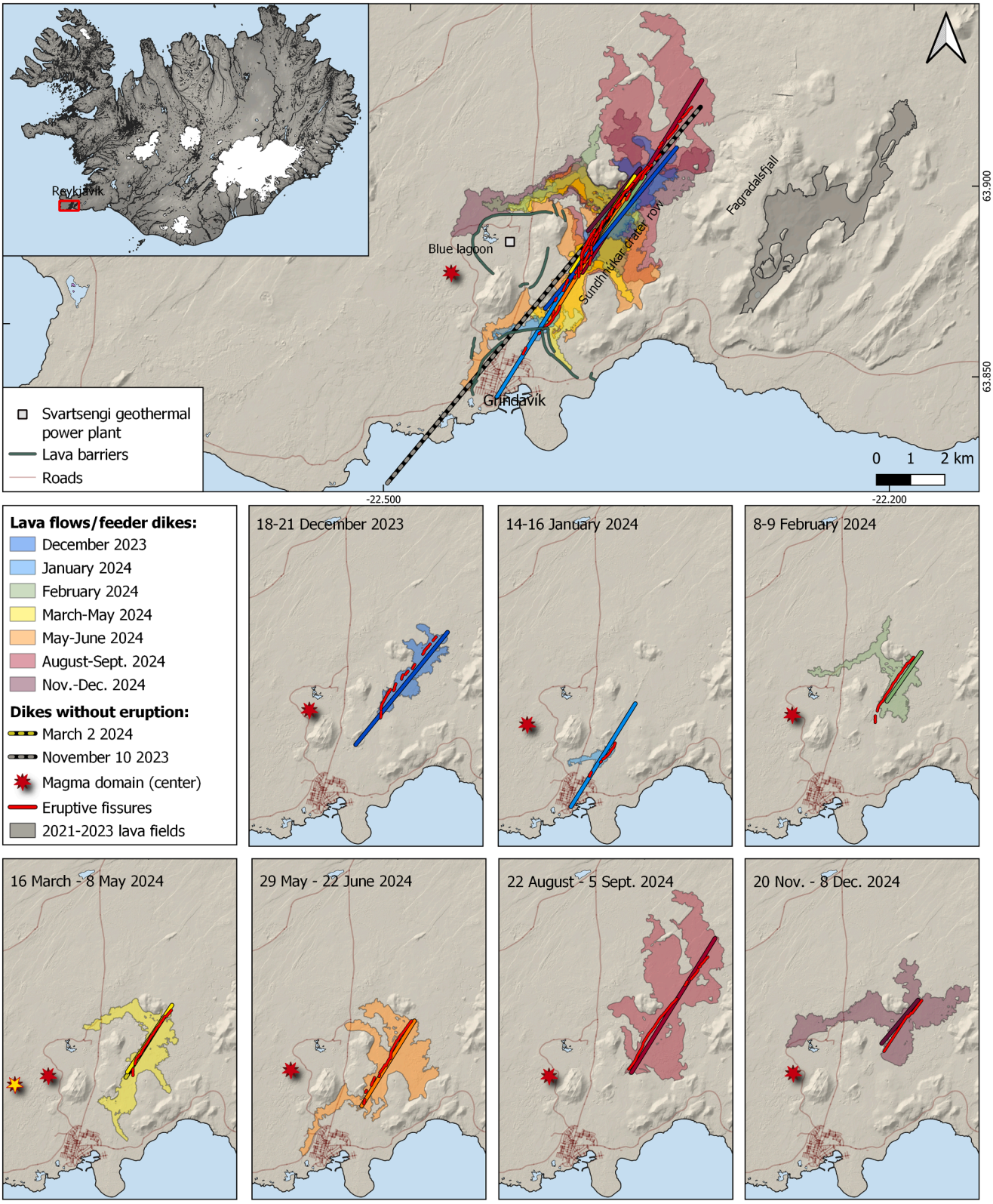

Fig. 2. Dike intrusions and eruptions in the Sundhnúkur area in 2023–2024. Top panel shows all dikes and lava flows, colored differently with time (dikes and the corresponding lava field are in the same color). The 2021–2023 Fagradalsfjall lava flows are shown in grey. Dated panels show the time-evolution of the subsequent dike intrusions after the November 10, 2023 dike. Red star indicates the inferred center of deflation within the magma domain for each of these periods. The panel with the eruption from 16 March to 8 May 2024 includes two dikes, the former dike formed on 2 March 2024 (yellow dashed line) but did not result in an eruption. The yellow star indicates the center of deflation related to that dike intrusion.

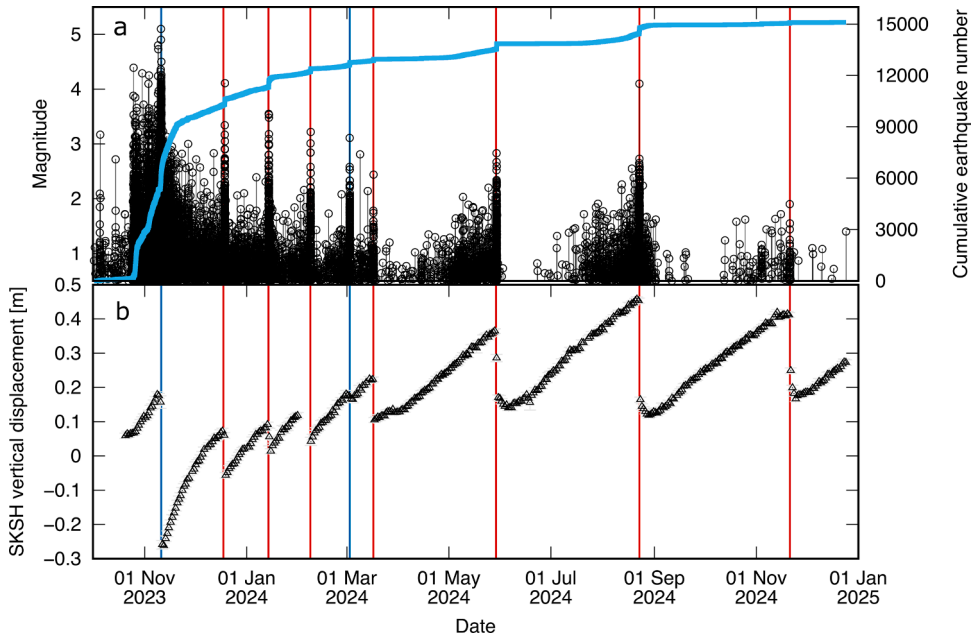

Fig. 3. Inflation-deflation episodes observed by GNSS time-series and seismicity within the diking area. (a) Seismicity timeline: Magnitudes (black) and cumulative number of earthquakes (blue) >M0.5, (b) Time-series of vertical displacement, at cGNSS station SKSH, located near the center of the inflation. See Fig. 2 for station location. Red vertical lines show onset of deflation events ending with an eruption, and blue vertical lines for diking events without an eruption.

approximately self-similar, fixed coordinates have been used for the point and sill sources in the automated models. Volume contraction of the magma domain during the diking events was also fixed using the results obtained from the joint InSAR and GNSS inversions (Table 1).

The cumulative opening associated with all the rifting events (diking events) in the period December 2023 until September 2024 was also estimated by using ascending and descending interferograms and GNSS observations bracketing the events. It is the only model presented here with the overall dike plane divided into patches and solving for opening on each; otherwise the models shown here are all with uniform opening on the dike plane, allowing also for uniform strike slip.

3. Results

3.1. Observed deformation and seismicity

From 27 October 2023 to 31 December 2024, geodetic measurements reveal ten periods of inflation and nine deflation events (Fig. 3). The seismicity was most intense during the initial hours of the dike intrusion on 10 November, when the crust was being ripped up by the intruding dike and stored tensional stress, releasing over 20 earthquakes of $M_W \geq 4$ in the diking area, including one $M_W 5.2$ at Mt. Hagafell (Sigmundsson et al., 2024); then gradually decaying over the following weeks. The eight subsequent dike intrusions generated much less seismicity, including only two $M_W 4$ events (in December 2023 and August 2024) and thus constituted a much lower seismic hazard than that experienced on 10 November 2023. In general, temporal characteristics of the seismicity accompanying the intrusions/eruptions, show a decrease in seismicity after the January (second) eruption, regarding both magnitudes and number of events. Although with the sixth eruption, in August, the seismicity appeared to increase again, but the most recent dike intrusion to date on 20 November 2024 was accompanied by very little seismicity. As the seismicity decreased, the short-term precursory time to eruption also decreased, requiring adjustment of the seismic alert monitoring procedures at IMO. The precursory activity consisted mostly of very small microearthquakes located near the center of the diking area between Mt. Stóra-Skógfell and Mt. Sundhnúkur, followed by stronger seismicity during dike propagation, both laterally and to the surface, usually ceasing soon after the onset of the eruptions (Fig. 3). Seismicity and deformation rates show a highly non-linear correlation. Seismicity is low following deflation events and increases only significantly after the previous level of inflation is reached, as observed for part of the Krafla Fires rifting episode and explained by the Kaiser effect (Heimisson et al., 2015).

Extensive series of GNSS observations (e.g. Fig. 3 & Supplementary Figure S1) and interferograms (Figs. 4 and 5 & Supplementary Figure S2) are available to study the events. The spatial pattern of ground deformation for each of the inflation episodes displays uplift and outward movement from the center of the magma domain on the GNSS observations, and a circular inflation pattern observed on InSAR. The GNSS timeseries clearly show the onset of each the diking event – indicated by rapid subsidence (e.g. Fig. 3 & Supplementary Figure S1). During each of these events, the InSAR shows a characteristic deformation pattern related to a dike intrusion (wing-shaped lobes on either side of the dike path related to both horizontal extension and uplift) and also deflation over the Svartsengi magma domain. The dike lobes interfere to different extents with the deflation signal, depending on the location and opening of the dikes.

3.2. Geodetic modelling: inflation periods

Time-series of inferred volume change, and the rate of volume change, of the Svartsengi magma domain is shown in Fig. 6, for a point source of pressure with a fixed depth of 4 km (average depth derived from joint InSAR and GNSS inversions). Corresponding results for a rectangular sill source with a fixed depth of 4.35 km are shown in Supplementary Figure S3. These results for the inflation periods are based on GNSS data only, with their reliability confirmed by a comparison of inflation deformation models using both GNSS and InSAR data (e.g. Fig. 7a, Supplementary Figures S4 & S5). The Mogi source typically provides a better-fit to the magnitude of the deformation signal during these events, despite not capturing the elongation of the signal in the NE-SW direction observed from InSAR. Joint inversions of InSAR and GNSS data spanning the inflation events using the sill source, placed the average top depth of the sill at 4.7 km, however these models consistently overestimated the vertical displacements (see

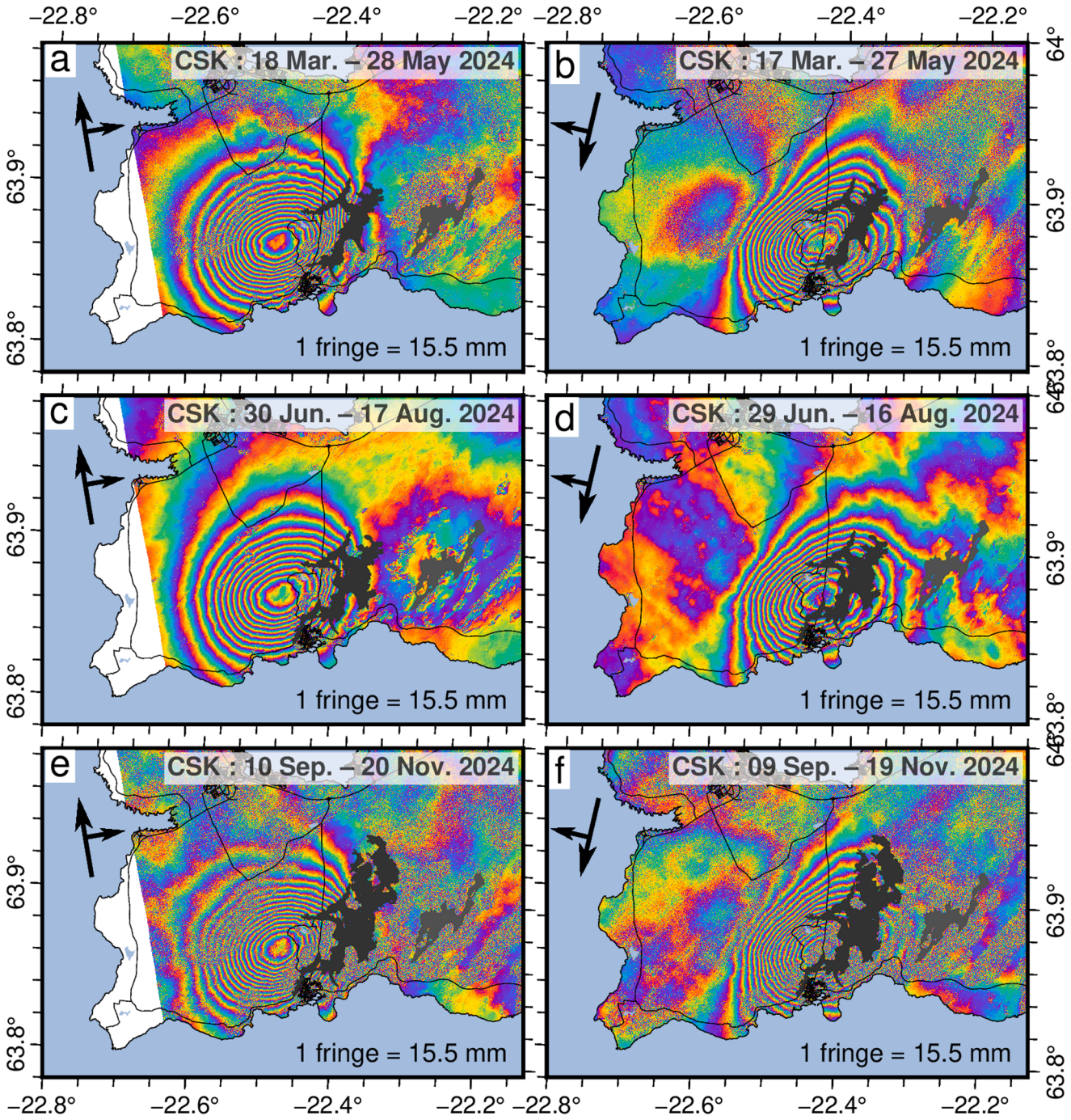

Fig. 4. Spatial pattern of deformation during inflation episodes as revealed by InSAR: selection of wrapped ascending (left column) and descending interferograms (right column) between March to November 2024. Interferograms based on data from the COSMO-SkyMed (CSK) satellites. Black arrows on each panel show satellite flight direction and look angle. One fringe of color corresponds to displacement in the line-of-sight (LOS) equal to half the wavelength of the satellite; shown at bottom left in each panel. Incoherent areas (where color fringes are not visible) are most pronounced in the winter months when snow was on the ground. Black shaded areas show the location and evolution of the Svartsengi lava fields during 2024 and in grey the Fagradalsfjall 2021-2023 lava fields.

Supplementary Figure S5). To compensate for this, the depth of the sill source was set here to 4.35 km for the automated modelling.

3.3. Geodetic modelling: diking events and co-eruptive deformation

Deformation models for co-diking and associated deflation source have used joint GNSS and InSAR inversions. The following section provides an overview of the results obtained from the optimal uniform opening dike models shown in Fig. 7b and Supplementary Figures S6 to S13. For source locations see Figs. 1 and 2, and for an overview and dike volumes see Table 1.

3.3.1. 18–19 December 2023 dike

The dike intruded in an area from Mt. Hagafell towards ~1 km northeast of Mt. Stóra-Skógfell and was about 6 km long. Model opening is ~1.2 m, confined to the upper 1.7 km of the crust. The dike strike is N36°E, similar strike to the 10 November 2023 dike (Sigmundsson et al., 2024). It likely used pre-existing pathways formed during that event but intruded to a shallower level.

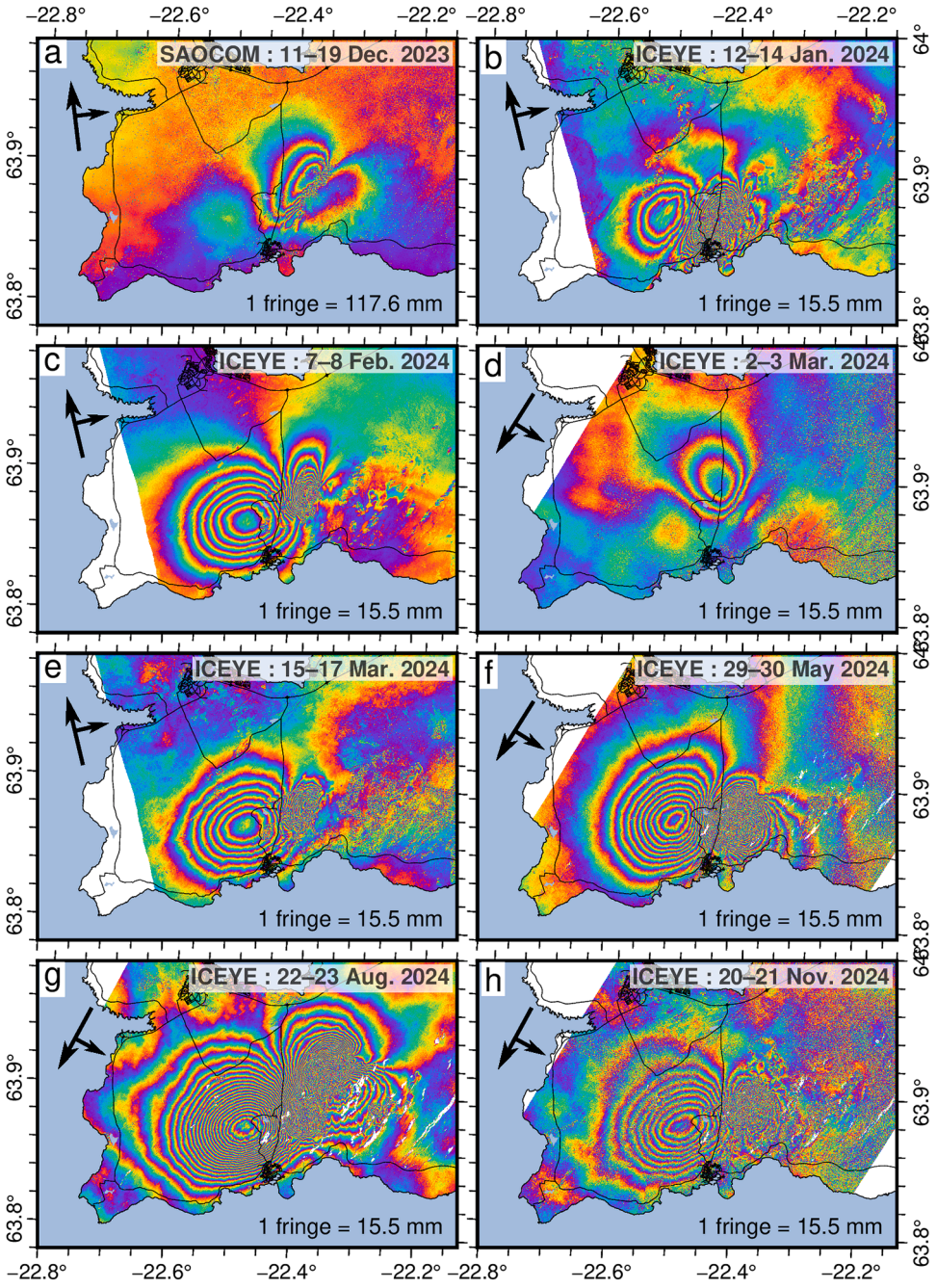

Fig. 5. Ground deformation in relation to deflation events and dike intrusions for the eight rifting events following the 10 November 2023 diking, as revealed by InSAR. Interferograms using data from the SAOCOM and ICEYE. Black arrows on each panel show satellite flight direction and look angle. One fringe of color corresponds to displacement in the line-of-sight (LOS) equal to half the wavelength of the satellite; shown at bottom left in each panel.

3.3.2. 14 January 2024 dike

The dike started from an area east of Mt. Sýlingarfell at the SW end of the Sundhnúkur crater row, from a likely turning point in the 18–19 December 2023 dike and then trended to the SW and propagated beneath the town of Grindavík. The dike is about 5 km long and has a strike of N29°E. It carved a new pathway compared to the previous dikes and caused a new graben subsidence in the eastern part of Grindavík. During this event an eruptive fissure opened on the northern edge of the town, which issued lava flows that destroyed three houses. This fissure lies directly above the path of the dike. Graben subsidence in the town of Grindavík is e.g. witnessed by difference in digital elevation models before and after the event (Supplementary Figure S14). The geodetic model has ~1.5 m opening from the surface to a depth of 3.3 km.

3.3.3. 8 February 2024 dike

The dike intruded on 8 February 2024 was about 2.5 km long located between Mt. Stóra-Skógfell and the SW end of the Sundhnúkur crater row, along a similar path as the northern segment of the December dike. Its SW end is at the point where the January dike commenced propagating (east of Sýlingarfell). The model has ~0.7 m opening in the upper 2.2 km of the crust, on a plane that strikes N32°E.

3.3.4. 2 March 2024 dike

A small dike intrusion, about 3 km long, occurred on 2 March 2024 which did not culminate in an eruption. The intrusion occurred from an area just east of Stóra-Skógfell towards ~1 km SE of Sýlingarfell – essentially a northern extension of the January dike. The optimal model

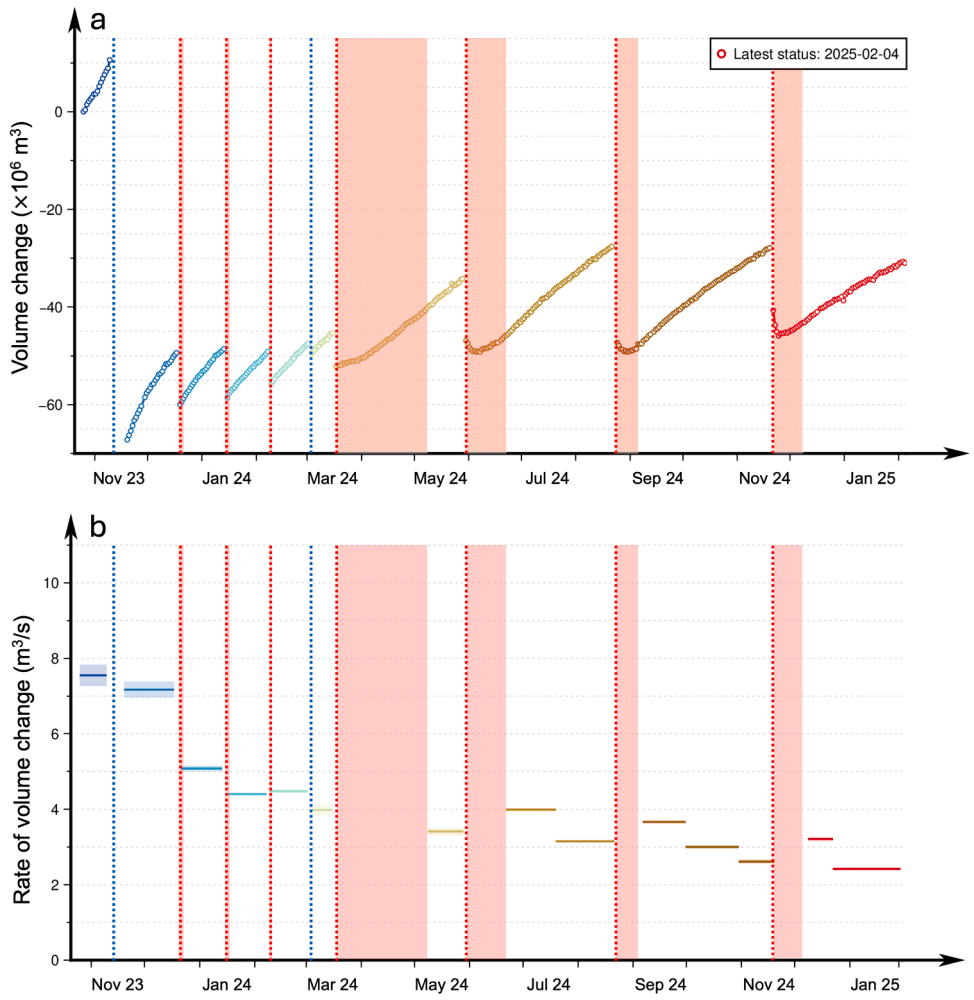

Fig. 6. Timeseries of volume change (a) and rate of volume change (b) within the Svartsengi magma domain since 25 October 2023. Results shown here use a point source of pressure (Mogi, 1958) to model the inflation and deflation episodes. Blue dashed lines indicate diking events that did not culminate in an eruption, red lines those that did. The pink shaded rectangles indicate the eruptive periods. The point source is located at −22.454°E, 63.869°N and depth 4 km.

has ~0.7 m opening in the 1.4–2.9 km depth range, on a plane that strikes N29°E, the same as the January dike.

3.3.5. 16 March 2024 dike

On the 16 March the Svartsengi magma domain failed again, resulting in the propagation of a 3.4 km long dike. Model opening is ~0.5 m in the uppermost 0.9 km of the crust. This intruded in the same location as the 2 March dike but migrated to a shallower level and extended about 700 m further to the NE.

3.3.6. 29 May 2024 dike

This dike was 4.2 km long, extending from south of Mt. Hagafell to the southern end of Mt. Stóra-Skógfell. It appears to have used a similar migration pathway as the January and March dikes. Model opening is ~0.8 m in the uppermost 1.3 km, on a plane striking N28°E.

3.3.7. 22–23 August 2024 dike

This dike intrusion was the largest since January, accompanied by the largest volume drop in the magma domain since the 10 November 2023 event. The dike was 6.7 km long and intruded within the upper 1.1 km. The strike was 28° and opening 0.8 m. This took a similar path as the February dike but extended significantly further to the NE by 3.3 km (0.7 km further to the NE than the 10 November dike).

3.3.8. 20–21 November 2024 dike

This diking event was the smallest so far in the sequence and associated with very little seismicity compared to prior events. The dike was 2.3 km long with a strike of 38° and opening of ~0.7 m. Magma was intruded in the uppermost 0.5 km of the crust.

3.3.9. Cumulative dike opening December 2023–August 2024

To determine the cumulative amount of opening along the dike complex between December 2023 - August 2024, an inversion was run using two SAOCOM interferograms (Supplementary Figure S15), and cumulative GNSS displacements covering the same period. The model includes a two-segment dike with a turning point close to the center of the Sundhúkur crater row (Supplementary Figure S16). The initial inversion comprised two sources – a deflating point source of pressure for the Svartsengi magma domain and a vertical Okada dislocation divided into patches to model distributed opening along the dike. The dike is 14 km long and patch size is 250 × 250 m between the surface and 1.5 km depth then 500 × 500 m from 1.5 to 3 km depth. The median distributed opening inferred with our modified version of the GBIS software is displayed in Supplementary Figure S17. It shows maximum cumulative opening between Mt. Hagafell to Mt. Stóra-Skógfell. However, shallow opening is also observed up to 1.5 km to the NE of Stóra-Skógfell and in the SW extending 750 m beneath the center of Grindavík.

To determine whether the shallow opening here may be affected by fault movement during the graben formation on 14 January 2024, we

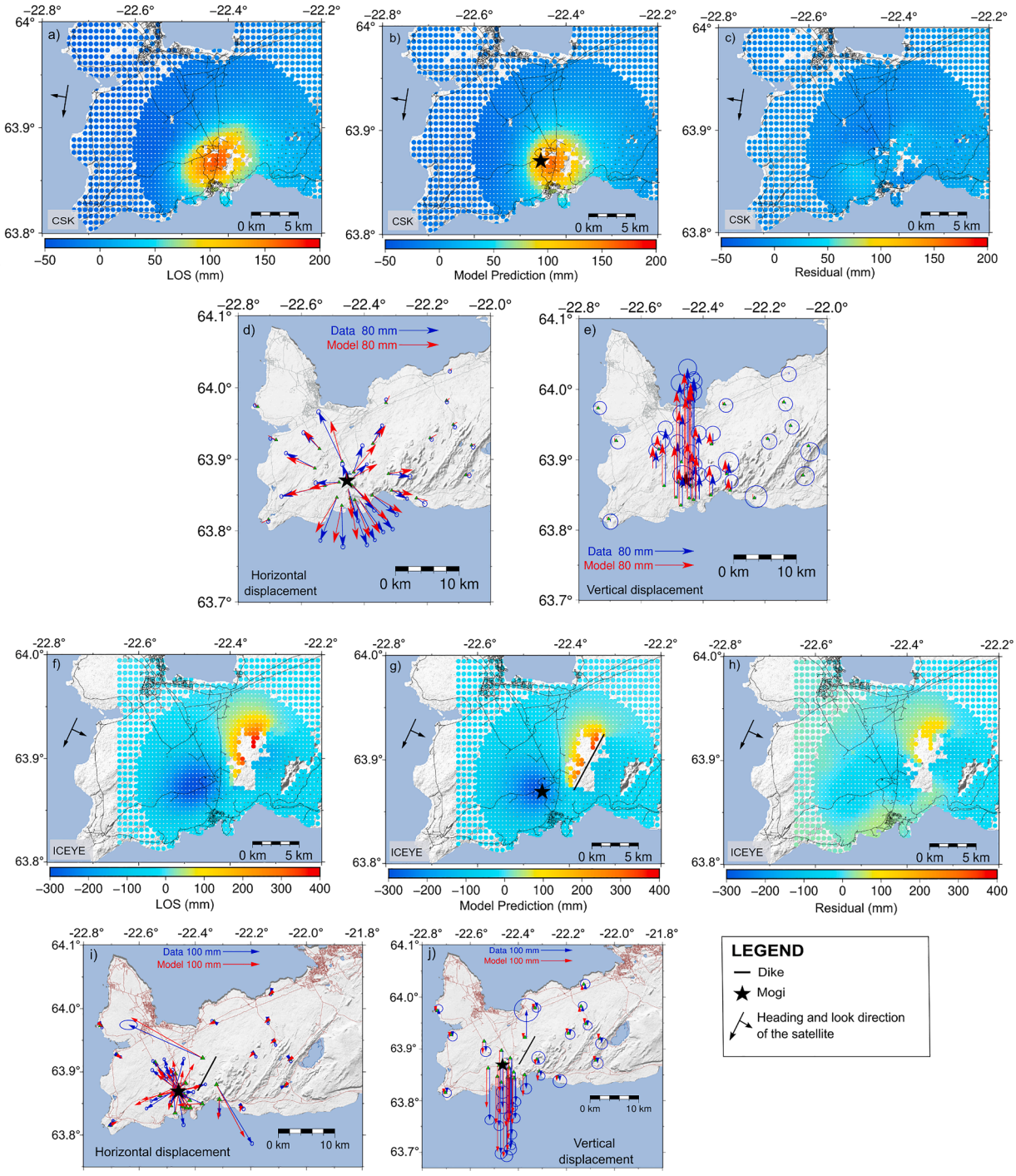

Fig. 7. Geodetic models using a point source of pressure (Mogi, 1958). (a-e) Geodetic model of Svartsengi inflation between 29 June to 17 August 2024. (a) LOS displacements for CSK descending interferogram (time period: 29 June – 16 August 2024), (b) best-fit model predictions and (c) residuals. (d) Horizontal GNSS displacements (blue) and modelled displacements (red). (e) Vertical GNSS displacements (blue) and modelled displacements (red). The black star in (b), (d) and (e) shows the location of the inflating point source. The corresponding model using a rectangular sill source is shown in Supplementary Figure S5. (f-j) Geodetic model of Svartsengi deflation and diking event on 22–23 August 2024. (f) LOS displacements for ICEYE descending interferogram (time period: 22–23 August 2024), (g) best-fit model predictions and (h) residuals. (i) Horizontal GNSS displacements (blue) and modelled displacements (red). (j) Vertical GNSS displacements (blue) and modelled displacements (red). The black line in (g), (i) and (j) shows the location of the dike and black star the location of the deflating point source. Green triangles in (d), (e), (i) and (j) show location of continuous GNSS stations. Probability density functions and details of modelled parameter ranges are displayed in Supplementary Figures S4 and S12.

ran a second model incorporating the two main graben faults inferred from comparison of digital elevation models as described in methods (Supplementary Figure S14). The maximum subsidence revealed by the elevation difference was 1.1 m of lowering at the NE-end of the January 2024 lavas, near Mt. Hagafell. Subsidence of 0.5 m was observed "en echelon" on the southern part of the January 2024 lavas and on the eastern side of Grindavík. Using this information, faults were incorporated on each side of the graben into the models as Okada dislocations dipping inwards toward the dike at 60°, allowing for both strike-slip and dip-slip motion and extending from the surface to a depth of 500 m

(Supplementary Figure S18). The result displayed in Fig. 8 shows a very similar pattern of opening as in a model with no faults (Supplementary Figure S17), indicating the shallow opening beneath Grindavík is not an artifact but a result of the magma intrusion on 14 January.

4. Discussion

The models presented here broadly explain the overall observed deformation pattern. Both point source of pressure and sill models have here been used to fit observations, whereas the real geometry of the inflation-deflation source may likely be of an ellipsoidal shape (Sigmundsson et al., 2024). The inferred eastern edge of it is in close proximity to the Sundhnúkur crater row, and failure has been occurring there. This, together with a tectonic setting within a highly oblique spreading zone, may explain the peculiar geometric arrangement of a magma domain located to the side of a fissure swarm where eruptions have occurred.

Deformation during deflation events is a combination of pressure drop in a localized source, and diking, influencing observations at GNSS stations to a varying degree. Although GNSS observations at an individual station show the key aspect of activity (Fig. 3), a clearer pattern is revealed when the whole geodetic data are inverted for change of volume of the Svartsengi magma domain (Fig. 6). Rates of volume change have decreased from the beginning of activity from ~7–9 m^3/s, to ~2.4–4 m^3/s in the May 2024–January 2025 period. During each inflation period, there is tendency for the inflow rate to decrease as the pressure builds within the magma domain. An additional process not taken into consideration here is revealed in residuals between observed ground deformation and models for some of the inflation periods, that give hints for some seeping of magma into the dike complex. However, small volumes are involved, and this is secondary to the processes described here. The data set presented here is superior compared to that available for earlier rifting episodes (e.g. Wright et al., 2012), and inference on the details of the magma plumbing system therefore less uncertain than in previous cases. Evaluation of forecasting of diking events and eruptions can be tested against well-observed repeated events.

4.1. Magma plumbing system

The interpretation of geochemistry of a dynamic mid-crustal magma domain (Matthews et al., 2024) fits well with our geodetic observations and interpretations, as well as earlier interpretations (Sigmundsson et al., 2024), considering uncertainty of each of the approaches used. Even if we find deformation of the inflation episodes to be broadly self-similar, detailed comparison of inflation episodes is suggestive of some differences in geometry and location of the inflation source, consistent with recharge of individual magma units within the magma domain. Failure and magma outflow from the magma domain has for all diking/eruptions occurred in a similar area, at the eastern edge of the inferred magma domain.

During the 10 November 2023 dike injection, the estimated peak magma inflow rate to the dike was over 7000 m^3/s (Sigmundsson et al., 2024). On 18 December 2023, the Svartsengi magma domain reached again critical pressure and this time triggered an additional rapid dike opening extending to the surface. An eruption began with rapid onset – preceded by only a 1.5 h long seismic swarm. The inferred peak magma inflow rate into the dike at this time was ~800 m^3/s. On 14 January another dike propagation occurred. This time it took a new path east of the 10 November dike and propagated beneath the center of the town of Grindavík.

On 2 March 2024, the magma domain failed once again triggering a small dike propagation lasting ~4 h, however this did not culminate in an eruption. The next dike propagation and eruption occurred on the 16 March. This eruption has been the longest to date, lasting 53 days and during which time both inflation of the Svartsengi magma domain and in the diking area was observed. Following a repose of 21 days, another dike propagation and eruption occurred on 29 May 2024 which continued until 22 June 2024. At the beginning of this event continued subsidence was observed in the Svartsengi magma domain during the first week of the eruption which then again changed to inflation despite the concurrent eruptive activity. On 22 August 2024, the magma domain failed once again. The associated volume loss in the magma domain was the largest since 10 November 2023 and the volume of erupted lava was also the largest to date. The smallest dike intrusion to date occurred on 20 November 2024, preceded by very little seismicity.

The summed median dike volume from November 2023 to November 2024 is 182×10^6 m^3 (Table 1), with >70 % of the inferred dikes volume emplaced in the first event. The total bulk lava volume of the eruptions on the Sundhnúkar crater row is $(217 \pm 13) \times 10^6$ m^3, as measured in December 2024 from photogrammetric methods. For comparison the summed median volume losses from the magma domain that led to volcanic eruptions is 159×10^6 m^3. This last number does not consider inflow into the system during eruptions. Multiple corrections are needed when comparing these numbers. An estimate of the volume loss from a magma domain is not the same as the volume of magma that flows out of it, because of the effects of magma compressibility of the magma domain (Sigmundsson et al., 2024). Furthermore, the bulk lava volume is significantly larger than the lava volume calculated as dry rock equivalent (DRE).

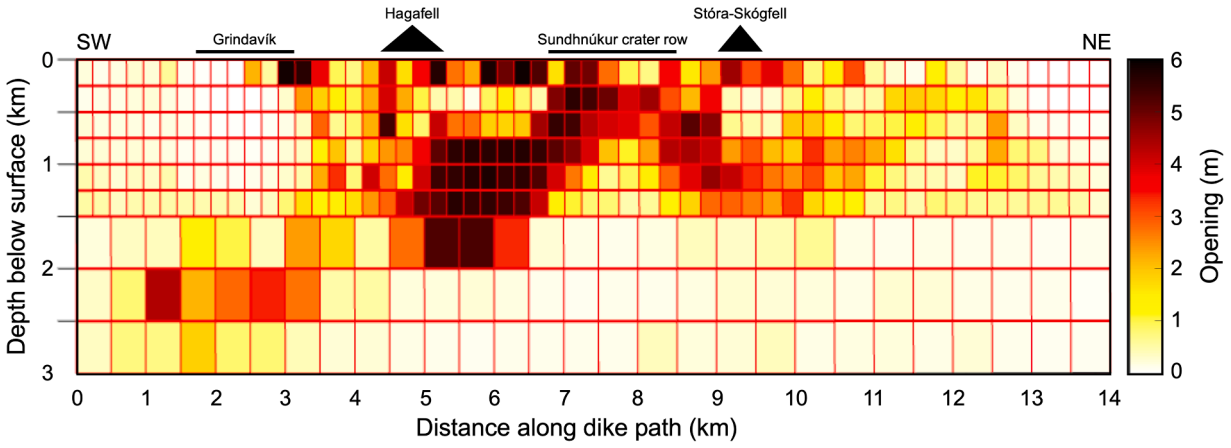

Fig. 8. Median distributed opening (color) in a geodetic model spanning the deflation and diking events that occurred between December 2023 to August 2024, using a point source of pressure for the magma domain, segmented dike divided into patches and two graben faults modelled as rectangular planes with constant slip (Okada, 1992). The dike path is shown in Supplementary Figures S16 & S18.

The main difference between the dike intrusions and eruptions thus far in the Svartsengi system and at the Fagradalsfjall system is how the magma accumulates prior to events and how it is migrating within the crust. At Fagradalsfjall, the magma was transferred from around 10–15 km depth (Halldórsson et al., 2022), feeding lateral dike intrusions in the upper crust between depths of ~1 to 6 km, without stopping in a mid-crustal magma domain. This explains the different style of activity within the two systems.

4.2. Forecasting

As soon as it was clear that the activity in Svartsengi did not switch off after the first eruption, the question was raised about when the following event would occur. Regular scientific meetings were held between scientists from different institutions, nationally and internationally, to constantly assess the situation considering the most recent observations, monitoring data and modelling results. The main effort was to try to determine the timeline for increased probability of the next diking event/eruption.

A tool which was used to gather scientists' expertise on a quantitative probability of a next event was the expert elicitation. Twelve elicitations were performed between 20 November 2023 and 23 May 2024, asking a variety of questions including the probability for a possible eruption within different time periods as well as its likely location within the Svartsengi area. Between 5 to 11 experts took part in the different elicitations. The last elicitation was done a week prior the eruption which commenced on 29 May 2024. Until then the results from the elicitations were formally adopted to assess the hazard within six different zones which were relevant for either critical infrastructure presence and exposed value or the spatial distribution of the ongoing activity. The elicitations were performed preferably after scientific meetings where scientists and experts had time to discuss together and elaborate on the current available data sets and interpretations (for more information see Supplementary Text S3).

In this process, a key role has been given to geodetic results. As deformation is affected by both deflation of the magma domain and the formation of a dike during each deflation event, the time-series of inflation/deflation volume from geodetic modelling have been used to evaluate the timing of the next eruption, rather than displacement trends at individual GNSS stations. Three somewhat different assumptions based on an inflation-predictable model (e.g., Segall et al., 2013) have been used to varying degrees during the series of events. When implementing them, a fixed geometry and location is used for the magma domain, and this causes some uncertainty.

The first approach hypothesized the next eruption would occur when the amount of volume increase in the magma domain following a sudden diking/eruption event equals the volume contraction in the previous event. This approach was used for forecasting diking events between 14 January to 2 March 2024, when it was estimated that the next event would occur once there was between (7–11) $\times 10^6$ m^3 volume recharge to the Svartsengi magma domain. On 2 March 2024, a small diking event occurred, within the anticipated timeframe considering this volume argumentation. However, it did not lead to an eruption. Following continued inflation for an additional 14 days, the next dike was triggered on 16 March 2024 which did result in an eruption.

The second approach was established to take into account that some eruptions are prolonged with inflation occurring during them. The first eruption of this type began on 16 March 2024 and before it ended on 8 May 2024 the amount of recharge was already more than the initial contraction volume. In the second approach the next eruption was forecast to occur when the volume increase of the magma domain after an eruption ended (when the system was closed) would equal the full contraction volume of the previous event (6.9×10^6 m^3). This approach was used to forecast the diking and eruption which occurred on 29 May 2024. Between 8 to 28 May 2024, we estimated a median recharge volume of 6×10^6 m^3 which is similar to the volume lost during the March 16 event (Supplementary Figure S19). The same technique was applied to forecast the likely timeframe for the following diking and eruption (Supplementary Figure S20). Then the median target volume was estimated at ~15×10^6 m^3 (modelled volume loss in reservoir on 29 May 2024 plus modelled volume change related to continued subsidence during the first week of the eruption, until 5 June 2024). Thereafter, considering only inflation since 22 June 2004 when the system was closed, the median target volume was expected to be reached by 9 August 2024. However the next diking event and eruption did not occur until 13 days later, on 22 August 2024.

Despite the correlation between volume contraction of the magma domain during the failure events and subsequent recharge during the closed system period (Supplementary Figure 21), applying the same technique to forecast the next event which occurred on 20 November 2024, indicated the lower bound would not be reached until 3 days after the event occurred, so the forecast date was too late (Fig. 9).

The third approach is to consider the total volume contraction of the magma domain versus total recharge from the local minimum on the inflation-deflation volume curve (e.g. total volume loss on 22 August 2024 plus the continued drop until 30 August 2024, which is about 22×10^6 m^3 for the August event). This technique would have been successful in forecasting the date of the diking and eruption onset on 20 November 2024 (Fig. 9) but would not have been able to successfully forecast the two events prior to 20 November 2024 (Supplementary Figures S19-S22).

Lessons learnt are that a forecasting technique needs to evolve based on the latest available data and models, and to take into consideration potential changes within the magma plumbing system. The significant uncertainties related to this should propagate into the forecasting. Since the 20 November 2024 event, IMO eruption forecasting continues to use the estimated volume contraction in a prior event as a proxy for the recharge volume increase required to trigger the next event but based on which of the approaches presented above predicts the earliest date a lower bound volume will be reached. For Svartsengi the behavior of the system changed in March 2024; before then failure occurred at a significantly lower level than after (Fig. 6 & Supplementary Figure 3). The 2 March event that did not culminate in an eruption, may indicate a change within the magma plumbing system. An explanation could be that the previously formed pathways from the Svartsengi magma domain into the diking area had started to solidify and a higher pressure increase/recharge volume was required.

Alongside medium-term forecasting, IMO uses early-warning systems and a designated contingency plan to activate when a dike has likely started propagating and an eruption may be imminent. Such warning systems are based on four main real-time monitoring indicators: i) level of seismicity (a specific number of earthquakes within a specific time window in a specific area, and sometimes above a specific magnitude), ii) changes in pressure in geothermal boreholes in the Svartsengi geothermal field (monitoring designed, maintained and automatic alarm issued by HS Orka energy company), iii) rapid deformation detected on real-time GNSS observations, and iv) changes in strain rate as detected on fiber optic cable (warning system designed by colleagues at Reykjavík University and California Institute of Technology, see Li et al., 2024). As soon as a warning has been activated, IMO personnel on duty interprets the real time data and proceed according to the contingency plan to activate emergency response and trigger actions by civil protection authorities. The effective warning time for the eruptions so far has ranged from 21 min to 4 h and 37 min.

4.3. Hazards

On 10 November 2023 seismic and geodetic measurements showed that a dike propagated beneath Grindavík, necessitating urgent evacuation of the town inhabitants. Major damage to infrastructure occurred, in particular because of ground fracturing within the town (De Pascale et al., 2024), the most extensive in Iceland since the Krafla rifting

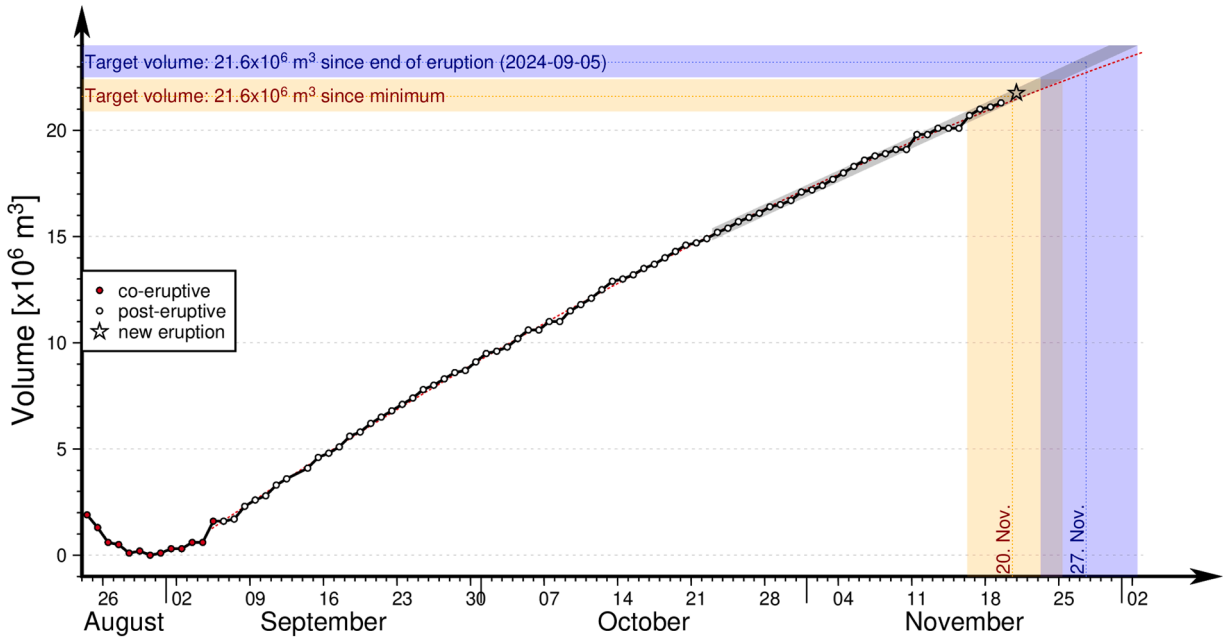

Fig. 9. Forecast for 20 November 2024 diking event and eruption. The blue shaded region shows the forecast assuming the next eruption will occur when the volume increase within the magma domain after an eruption ended (when the system was closed) equals the full contraction volume of the previous event. The orange shaded region illustrates an alternate forecasting approach in which the eruption is expected to happen when the total recharge equals the total contraction volume of the previous event. Dots within the time-series show inferred volume change from GNSS observations. The grey shaded region indicates the 95 % prediction interval of the linear regression fit using the last 4 weeks of inflation. The dashed red line shows a second-degree polynomial fit using all the post-eruptive data points. The trend of volume change evolution allows an estimate of the likely time interval for the next event, where this intersects the lower and upper bounds of the orange and blue regions. The zero point on the y-axis is set to the minimum of the volume drop observed following the onset of the diking event.

episode in North Iceland 1975–1984 (e.g., Hjartardóttir et al., 2012). A second dike propagation, this time associated with opening of an eruptive vent, occurred within the town of Grindavík on 14 January 2024, and caused more destruction. In addition to the lava flows that destroyed three houses, it was ground fracturing and fissure openings that caused significant damage, as houses had been built on active faults. In light of this, the town of Grindavík still remains a danger zone. The ongoing period of activity has seriously disrupted the life of the people in the town of Grindavík, resulting in relocation of the majority of the prior ~3600 residents and closure of businesses.

Eruption hazards are a major concern because of the close proximity to the town of Grindavík, the Svartsengi power plant, critical infrastructure and the Blue Lagoon geothermal resort that is very popular with tourists. Expected future eruptive activity is similar as previous, main hazards relate to fast effusive eruptions of lava flows and gas pollution near inhabited areas, causing major risk to people and infrastructure. Shaking due to earthquakes is also a concern, although the seismicity associated with eruptions has been decreasing. It has been inferred that the outflow path from the Svartsengi magma domain has a relatively large cross-sectional area (Sigmundsson et al., 2024), facilitating rapid magma flow to shallow levels in the crust and to the surface. As more pressure seems to be able to build up prior to the later eruptions (compared to earlier eruptions between December 2023 to March 2024), there is need to be prepared for larger eruptions than those which have occurred so far in the area.

A major operation to mitigate the effects of lava flows has been the construction of barriers to divert lava flows. Construction of lava barriers to protect the Svartsengi powerplant began on 15 November 2023, only five days after the 10 November 2023 diking event. Such rapid response was facilitated by prior testing of building and use of lava barriers during the eruptions at Fagradalsfjall in 2021–2023. Construction of barriers around Grindavík began on 29 December 2023, and throughout 2024 barrier construction has continued (see Fig. 1 & Supplementary Figure S16). Lava has been diverted by the barriers in the January, March, May and November eruptions in 2024. Subsequently, barriers have been heightened in response to lava building up at these, and in some instances where it has breached the barriers. As of end of January 2025 the height of lava barriers above surroundings was between 3 and 24 m, built to have a significant effect of diverting lava in future eruptions both from the Svartsengi power plant and the town of Grindavík. This assumes lava flows on the surface, although it is possible that magma may flow laterally in fractures at shallow depth under the existing lava barriers, thereby reaching Grindavík.

If more dike propagations occur in the near-future, it is considered most probable that pre-existing magma pathways will guide the dikes into the area similar as in the previous events, however formation of dikes in other parts of the volcanic system cannot be excluded. Regarding future activity on the Sundhnúkur crater row and its extension, it is challenging to estimate where future diking and eruptions are most probable. The eruptive fissure that opened on 22 August 2024 was the northeastern most of the fissures that have opened so far. However, in November 2024 the activity switched again to the central part of the Sundhnúkur crater row. Future events may again move further to the northeast or to the southwest (closer to the town of Grindavík). The distributed opening model for the average dike path for the dikes intruded between December 2023 to August 2024, shows the maximum cumulative opening occurs in the region between Hagafell and Stóra-Skógfell. This region of the Sundhnúkur crater row is closest to the Svartsengi magma domain and may still be the preferred pathway to facilitate future magma migration, as was observed during the most recent eruption in November 2024.

5. Conclusions

A rifting episode began on 10 November 2023 in the Svartsengi volcanic system, SW-Iceland, with an initial diking event, following episodic inflation there since January 2020. These inflation events relate to recharging of a magma domain, at a geodetically inferred depth of

4–5 km, assuming a model with a deformation source within a uniform elastic half-space. The initial rifting event has been followed by eight additional events until November 2024, causing centimeter to meter scale deformation registered by GNSS and InSAR, ground fracturing and eruptions associated with seven of them. Deformation and seismicity during deflation events can be explained in terms of a combination of a simple source of pressure decrease in a magma domain, concurrent with magma intrusion into vertical dikes up to 15 km long at the Sundhnúkur crater row. Geodetic inversion considering graben faults suggest movement on them is limited to the top layer of the crust, and at depth most crustal widening can be attributed to dike opening. Continuous inflation has occurred between the diking events, with rate of volume increase of the Svartsengi magma domain amounting initially to ~7–9 m^3/s but declining to ~2.4–4 m^3/s. Timing of diking events and eruptions have been forecast based on different approaches using the anticipated correlation between volume contraction during deflation periods and subsequent volume recharged to the system before the next event is triggered.

CRediT authorship contribution statement

Michelle Parks: Writing – review & editing, Writing – original draft, Methodology, Investigation, Formal analysis, Conceptualization. **Vincent Drouin:** Writing – review & editing, Validation, Software, Methodology, Investigation, Formal analysis. **Freysteinn Sigmundsson:** Writing – review & editing, Writing – original draft, Methodology, Conceptualization. **Ásta R. Hjartardóttir:** Writing – review & editing, Visualization, Formal analysis. **Halldór Geirsson:** Writing – review & editing, Visualization, Formal analysis. **Gro B.M. Pedersen:** Writing – review & editing, Formal analysis. **Joaquin M.C. Belart:** Writing – review & editing, Visualization, Formal analysis, Conceptualization. **Sara Barsotti:** Writing – review & editing. **Chiara Lanzi:** Writing – review & editing, Visualization, Formal analysis. **Kristín Vogfjörd:** Writing – review & editing, Methodology, Investigation. **Andrew Hooper:** Writing – review & editing, Software, Methodology. **Benedikt Ófeigsson:** Writing – review & editing, Methodology, Formal analysis. **Sigrún Hreinsdóttir:** Writing – review & editing, Methodology, Formal analysis. **Einar Bessi Gestsson:** Writing – review & editing. **Ragnar H. Þrastarson:** Writing – review & editing, Visualization. **Páll Einarsson:** Writing – review & editing. **Valentyn Tolpekin:** Writing – review & editing, Methodology, Formal analysis. **Drew Rotheram-Clarke:** Writing – review & editing, Methodology, Formal analysis. **Sydney R. Gunnarsson:** Writing – review & editing, Methodology, Formal analysis. **Birgir V. Óskarsson:** Writing – review & editing, Methodology, Investigation. **Virginie Pinel:** Writing – review & editing, Methodology, Investigation.

Declaration of competing interest

The authors declare no conflict of interest.

Acknowledgements

We would like to thank the editor and an anonymous reviewer for their constructive feedback which helped to significantly improve this manuscript. Thanks to all Icelandic Meteorological Institute (IMO) staff involved in the routine monitoring of the Reykjanes Peninsula, and IMO and University of Iceland technicians for support and operation of the seismic and GNSS stations. Thanks also for support from, and extensive discussions, with many scientists at IMO, University of Iceland, HS Orka, Reykjavík University, Natural Science Institute of Iceland, and the Icelandic Civil Protection. Earthquake detections and locations on Reykjanes Peninsula are substantially improved by data from eight additional stations owned by the Czech Academy of Sciences and operated by the Iceland GeoSurvey, two additional stations operated in collaboration between the Iceland Geosurvey and IMO, and one station owned by the University of Cambridge. This research was supported by the Icelandic Research Fund (grant numbers 228933–051 and 239615–051), the University of Iceland Research Fund and the H2020 DEEPVOLC project, funded by the European Research Council (grant number 866085) and the UK Natural Environment Research Council (NERC) through the Centre for the Observation and Modelling of Earthquakes, Volcanoes and Tectonics (COMET). The photogrammetric surveys were done using the aerial system PhaseOne iXM-100, funded by the Icelandic Infrastructure Fund (project number 232792–901) and the flights were funded by the Icelandic Civil Defense. Pléiades images were acquired as a response to the first dike intrusion on 10 November 2023. They were collected daily for ten consecutive days, thanks to the CNES via **CIEST^2** (© CNES **2023**, Distribution Airbus DS). **CIEST^2** is part of **FormaTerre** (https://en.poleterresolide.fr/) and supported by ISDeform National Observation Service. We thank the GEO Geohazard Supersites and Natural Laboratory (GSNL) Icelandic Volcanoes Supersite project supported by the Committee on Earth Observing Satellites for providing access to satellite data that was utilized in this study.

Supplementary materials

Supplementary material associated with this article can be found, in the online version, at doi:10.1016/j.epsl.2025.119324.

Data availability

Data will be made available on request.

References

Altamimi, Z., Métivier, L., Collilieux, X., 2012. ITRF2008 plate motion model. J. Geophys. Res. 117, 2011JB008930. https://doi.org/10.1029/2011JB008930.

Antonioli, A., Belardinelli, M.E., Bizzarri, A., Vogfjord, K.S., 2006. Evidence of instantaneous dynamic triggering during the seismic sequence of year 2000 in south Iceland. J. Geophys. Res. 111, 2005JB003935. https://doi.org/10.1029/2005JB003935.

Árnadóttir, T., Geirsson, H., Einarsson, P., 2004. Coseismic stress changes and crustal deformation on the Reykjanes Peninsula due to triggered earthquakes on 17 June 2000. J. Geophys. Res. 109, 2004JB003130. https://doi.org/10.1029/2004JB003130.

Bagnardi, M., Hooper, A., 2018. Inversion of surface deformation data for rapid estimates of source parameters and uncertainties: a bayesian approach. Geochem. Geophys. Geosyst. 19, 2194–2211. https://doi.org/10.1029/2018GC007585.

Barsotti, S., Parks, M.M., Pfeffer, M.A., Óladóttir, B.A., Barnie, T., Titos, M.M., Jónsdóttir, K., Pedersen, G.B.M., Hjartardóttir, Á.R., Stefansdóttir, G., et al., 2023. The eruption in Fagradalsfjall (2021, Iceland): how the operational monitoring and the volcanic hazard assessment contributed to its safe access. Nat. Hazards 116, 3063–3092. https://doi.org/10.1007/s11069-022-05798-7.

Björnsson, S., Einarsson, P., Tulinius, H., Hjartardóttir, Á.R., 2020. Seismicity of the Reykjanes Peninsula 1971–1976. J. Volcanol. Geotherm. Res. 391, 106369. https://doi.org/10.1016/j.jvolgeores.2018.04.026.

Böðvarsson, R., Rögnvaldsson, S.Th., Slunga, R., Kjartansson, E., 1999. The SIL data acquisition system—At present and beyond year 2000. Phys. Earth Planet. Inter. 113, 89–101. https://doi.org/10.1016/S0031-9201(99)00032-1.

Clifton, A.E., Kattenhorn, S.A., 2006. Structural architecture of a highly oblique divergent plate boundary segment. Tectonophysics 419, 27–40. https://doi.org/10.1016/j.tecto.2006.03.016.

Cubuk-Sabuncu, Y., Jónsdóttir, K., Caudron, C., Lecocq, T., Parks, M.M., Geirsson, H., Mordret, A., 2021. Temporal seismic velocity changes during the 2020 rapid inflation at Mt. Þorbjörn-Svartsengi, Iceland, using seismic ambient noise. Geophys. Res. Lett. 48. https://doi.org/10.1029/2020GL092265 e2020GL092265.

Dalkhani, A.R., Ágústsdóttir, T., Gudnason, E.Á., Hersir, G.P., Zhang, X., Weemstra, C., 2024. Transdimensional ambient-noise surface wave tomography of the Reykjanes Peninsula. SW Iceland Geophys. J. Int. 236, 621–643. https://doi.org/10.1093/gji/ggad435.

De Pascale, G.P., Fischer, T.J., Moreland, W.M., Geirsson, H., Hrubcová, P., Drouin, V., Forester, D., Payet–Clerc, M., Da Silveira, D.B., Vlček, J., et al., 2024. On the move: 2023 observations on real time graben formation, Grindavík, Iceland. Geophys. Res. Lett. 51, e2024GL110150. https://doi.org/10.1029/2024GL110150.

Ducrocq, C., Árnadóttir, T., Einarsson, P., Jónsson, S., Drouin, V., Geirsson, H., Hjartardóttir, Á.R., 2024. Widespread fracture movements during a volcano-tectonic unrest: the Reykjanes Peninsula, Iceland, from 2019 to 2021 TerraSAR-X interferometry. Bull. Volcanol. 86, 14. https://doi.org/10.1007/s00445-023-01699-0.

Einarsson, P., 2008. Plate boundaries, rifts and transforms in Iceland. Jök 58, 35–58. https://doi.org/10.33799/jokull2008.58.035.

Einarsson, P., 1991. Earthquakes and present-day tectonism in Iceland. Tectonophysics 189, 261–279. https://doi.org/10.1016/0040-1951(91)90501-I.

Flóvenz, Ó.G., Wang, R., Hersir, G.P., Dahm, T., Hainzl, S., Vassileva, M., Drouin, V., Heimann, S., Isken, M.P., Gudnason, E.Á., et al., 2022. Cyclical geothermal unrest as a precursor to Iceland's 2021 Fagradalsfjall eruption. Nat. Geosci. 15, 397–404. https://doi.org/10.1038/s41561-022-00930-5.

Geirsson, H., Parks, M., Vogfjörd, K., Einarsson, P., Sigmundsson, F., Jónsdóttir, K., Drouin, V., Ófeigsson, B.G., Hreinsdóttir, S., Ducrocq, C., 2021. The 2020 volcano-tectonic unrest at Reykjanes Peninsula, Iceland: stress triggering and reactivation of several volcanic systems. https://doi.org/10.5194/egusphere-egu21-7534.

Gouhier, M., Pinel, V., Belart, J.M.C., De Michele, M., Proy, C., Tinel, C., Berthier, E., Guéhenneux, Y., Gudmundsson, M.T., Óskarsson, B.V., et al., 2022. CNES-ESA satellite contribution to the operational monitoring of volcanic activity: the 2021 Icelandic eruption of Mt. Fagradalsfjall. J Appl. Volcanol. 11, 10. https://doi.org/10.1186/s13617-022-00120-3.

Guðjónsdóttir, S.R., Ilyinskaya, E., Hreinsdóttir, S., Bergsson, B., Pfeffer, M.A., Michalczewska, K., Aiuppa, A., Óladóttir, A.A., 2020. Gas emissions and crustal deformation from the Krýsuvík high temperature geothermal system. Iceland. J. Volcanol. Geotherm. Res. 391, 106350. https://doi.org/10.1016/j.jvolgeores.2018.04.007.

Halldórsson, S.A., Marshall, E.W., Caracciolo, A., Matthews, S., Bali, E., Rasmussen, M.B., Ranta, E., Robin, J.G., Guðfinnsson, G.H., Sigmarsson, O., Maclennan, J., et al., 2022. Rapid shifting of a deep magmatic source at Fagradalsfjall volcano, Iceland. Nature 609, 529–534. https://doi.org/10.1038/s41586-022-04981-x.

Heimisson, E.R., Einarsson, P., Sigmundsson, F., Brandsdóttir, B., 2015. Kilometer-scale Kaiser effect identified in Krafla volcano. Iceland Geophys. Res. Lett. 42, 7958–7965. https://doi.org/10.1002/2015GL065680.

Herring, T.A., King, R.W., Floyd, M.A., McClusky, S.C., 2018. GAMIT (GPS at MIT). Reference Manual Version 10.7. Department of Earth, Atmospheric, and Planetary Sciences. Massachusetts Institute of Technology, Cambridge, MA, USA.

Hjartardóttir, Á.R., Einarsson, P., Bramham, E., Wright, T.J., 2012. The Krafla fissure swarm, Iceland, and its formation by rifting events. Bull. Volcanol. 74, 2139–2153. https://doi.org/10.1007/s00445-012-0659-0.

Hreinsdóttir, S., Einarsson, P., Sigmundsson, F., 2001. Crustal deformation at the oblique spreading Reykjanes Peninsula, SW Iceland: GPS measurements from 1993 to 1998. J. Geophys. Res. 106, 13803–13816. https://doi.org/10.1029/2001JB000428.

Jenness, M.H., Clifton, A.E., 2009. Controls on the geometry of a holocene crater row: a field study from southwest Iceland. Bull. Volcanol. 71, 715–728. https://doi.org/10.1007/s00445-009-0267-9.

Jóhannesson, H., Sæmundsson, K., 2009. Geological map of Iceland 1:600,000. Tectonics.

Keiding, M., Árnadóttir, T., Jónsson, S., Decriem, J., Hooper, A., 2010. Plate boundary deformation and man-made subsidence around geothermal fields on the Reykjanes Peninsula. Iceland. J. Volcanol. Geotherm. Res. 194, 139–149. https://doi.org/10.1016/j.jvolgeores.2010.04.011.

Keiding, M., Árnadóttir, T., Sturkell, E., Geirsson, H., Lund, B., 2008. Strain accumulation along an oblique plate boundary: the Reykjanes Peninsula, southwest Iceland. Geophys. J. Int. 172, 861–872. https://doi.org/10.1111/j.1365-246X.2007.03655.x.

Li, J., Hjorleifsdottir, V., Biondi, E., Jonsdottir, K., Zhan, Z., 2024. Real-time monitoring and early warning of volcanic eruptions with low-frequency distributed acoustic sensing. In: Am. Geophys. Un., AGU annual meeting. https://agu.confex.com/agu/agu24/meetingapp.cgi/Paper/1703321.

Lyard, F., Lefevre, F., Letellier, T., Francis, O., 2006. Modelling the global ocean tides: modern insights from FES2004. Ocean Dyn. 56, 394–415. https://doi.org/10.1007/s10236-006-0086-x.

Martins, J.E., Weemstra, C., Ruigrok, E., Verdel, A., Jousset, P., Hersir, G.P., 2020. 3D S-wave velocity imaging of Reykjanes Peninsula high-enthalpy geothermal fields with ambient-noise tomography. J. Volcanol. Geotherm. Res. 391, 106685. https://doi.org/10.1016/j.jvolgeores.2019.106685.

Matthews, S.W., Caracciolo, A., Bali, E., Halldórsson, S.A., Sigmarsson, O., Guðfinnsson, G.H., Pedersen, G.B.M., Robin, J.G., Marshall, E.W., Aden, A.A., et al., 2024. A dynamic mid-crustal magma domain revealed by the 2023 to 2024 Sundhnúksgígar eruptions in Iceland. Science 386, 309–314. https://doi.org/10.1126/science.adp8778.

Mogi, K., 1958. Relation between the eruption of various volcanoes and the deformation of the ground surface around them. Bull. Earthq. Res. Inst. 36, 99–134.

Nuth, C., Kääb, A., 2011. Co-registration and bias corrections of satellite elevation data sets for quantifying glacier thickness change. The Cryosphere 5, 271–290. https://doi.org/10.5194/tc-5-271-2011.

Okada, Y., 1992. Internal deformation due to shear and tensile faults in a half-space. Bull. Seismol. Soc. Am. 82, 1018–1040. https://doi.org/10.1785/BSSA0820021018.

Pagli, C., Pedersen, R., Sigmundsson, F., Feigl, K.L., 2003. Triggered fault slip on June 17, 2000 on the Reykjanes Peninsula, SW-Iceland captured by radar interferometry. Geophys. Res. Lett. 30. https://doi.org/10.1029/2002GL015310, 2002GL015310.

Parks, M., Sigmundsson, F., Drouin, V., Hjartardóttir, Á.R., Geirsson, H., Hooper, A., Vogfjörd, K.S., Ófeigsson, B.G., Hreinsdóttir, S., et al., 2023. Deformation, seismicity, and monitoring response preceding and during the 2022 Fagradalsfjall eruption. Iceland. Bull. Volcanol. 85, 60. https://doi.org/10.1007/s00445-023-01671-y.

Parks, M., Sigmundsson, F., Sigurðsson, Ó., Hooper, A., Hreinsdóttir, S., Ófeigsson, B., Michalczewska, K., 2020. Deformation due to geothermal exploitation at Reykjanes, Iceland. J. Volcanol. Geotherm. Res. 391, 106438. https://doi.org/10.1016/j.jvolgeores.2018.08.016.

Pedersen, G.B.M., Belart, J.M.C., Óskarsson, B.V., Gudmundsson, M.T., Gies, N., Högnadóttir, T., Hjartardóttir, Á.R., Pinel, V., Berthier, E., Dürig, T., et al., 2022. Volume, effusion rate, and lava transport during the 2021 Fagradalsfjall eruption: results from near real-time photogrammetric monitoring. Geophys. Res. Lett. 49. https://doi.org/10.1029/2021GL097125 e2021GL097125.

Pétursson, G.G., Vogfjörð, K.S., 2009. Icelandic Meteorological Office report 1670-8261; VÍ 2009-012. https://www.vedur.is/media/vedurstofan/utgafa/skyrslur/2009/VI_2009_012.pdf.

Rögnvaldsson, S.Th., Slunga, R., 1993. Routine fault plane solutions for local networks: a test with synthetic data. Bull. Seism. Soc. Am. 83, 1232–1247. https://doi.org/10.1785/BSSA0830041232.

Sæmundsson, K., Jóhannesson, H., Hjartarson, Á., Kristinsson, S.G., Sigurgeirsson, M.Á., 2010. Geological Map of Southwest Iceland. Iceland Geosurvey.

Sæmundsson, K., Sigurgeirsson, M.Á., Friðleifsson, G.Ó., 2020. Geology and structure of the Reykjanes volcanic system, Iceland. J. Volcanol. Geotherm. Res. 391, 106501. https://doi.org/10.1016/j.jvolgeores.2018.11.022.

Segall, P., 2013. Volcano deformation and eruption forecasting. Geol. Soc. Lond. Spec. Publ. 380, 85–106. https://doi.org/10.1144/SP380.4.

Sigmundsson, F., Parks, M., Geirsson, H., Hooper, A., Drouin, V., Vogfjörd, K.S., Ófeigsson, B.G., Greiner, S.H.M., Yang, Y., et al., 2024. Fracturing and tectonic stress drive ultrarapid magma flow into dikes. Science 383, 1228–1235. https://doi.org/10.1126/science.adn2838.

Sigmundsson, F., Parks, M., Hooper, A., Geirsson, H., Vogfjörd, K.S., Drouin, V., Ófeigsson, B.G., Hreinsdóttir, S., Hjaltadóttir, S., Jónsdóttir, K., et al., 2022. Deformation and seismicity decline before the 2021 Fagradalsfjall eruption. Nature 609, 523–528. https://doi.org/10.1038/s41586-022-05083-4.

Sigmundsson, F., Einarsson, P., Hjartardóttir, Á.R., Drouin, V., Jónsdóttir, K., Arnadottir, T., Geirsson, H., Hreinsdottir, S., Li, S., Ofeigsson, B.G., 2020. Geodynamics of Iceland and the signatures of plate spreading. J. Volcanol. Geotherm. Res. 391, 106436. https://doi.org/10.1016/j.jvolgeores.2018.08.014.

Sigurgeirsson, M., 2023. Er vitað hversu mörg eldgos urðu á Reykjanesskaganum á síðasta eldgosatímabili? (in Icelandic: is it known how many eruptions occurred on the Reykjanes Peninsula in the last eruptive period). The Icelandic Web of Science. https://www.visindavefur.is/svar.php?id=81515 (last access: 11 November 2024).

Sturkell, E., Sigmundsson, F., Einarsson, P., Bilham, R., 1994. Strain accumulation 1986–1992 across the Reykjanes Peninsula Plate Boundary, Iceland, determined from GPS measurements. Geophys. Res. Lett. 21, 125–128. https://doi.org/10.1029/93GL03421.

Vadon, H., Sigmundsson, F., 1997. Crustal deformation from 1992 to 1995 at the Mid-Atlantic Ridge, Southwest Iceland, mapped by satellite radar interferometry. Science 275, 194–197. https://doi.org/10.1126/science.275.5297.194.

Wright, T.J., Sigmundsson, F., Pagli, C., Belachew, M., Hamling, I.J., Brandsdóttir, B., Calais, E., 2012. Geophysical constraints on the dynamics of spreading centres from rifting episodes on land. Nat. Geosci. 5 (4), 242–250. https://doi.org/10.1038/ngeo1428.